J Mol Model (2015) 21: 2
DOI 10.1007/s00894-014-2551-7

ORIGINAL PAPER

Effect of water in amorphous polyvinyl formal: insights from molecular dynamics simulation

Qiang Yin · Lin Zhang · Bo Jiang · Qinjian Yin · Kai Du

Received: 12 June 2014 / Accepted: 30 November 2014 / Published online: 22 January 2015

Abstract In this study, molecular dynamics simulations were performed to study the influence of water on polyvinyl formal. The effects of adding different concentrations of water (0, 0.23, 0.47, 0.94, 1.40, 1.86, 2.76, 3.65 and 4.52 wt%) to a copolymer of polyvinyl acetal, polyvinyl alcohol, and polyvinyl acetate were investigated. Simulated results clearly indicated that the radius of gyration of the polymer chain decreased whereas the cohesive energy density increased with the addition of water molecules. The diffusion coefficient initially decreased and then monotonically increased with increasing water concentration, and the same trend was observed for the fractional free volume. The results provide insights into the molecular structural and physical properties of polyvinyl formal with different water contents.

Keywords Polyvinyl formal · Water · Molecular dynamics simulation

Introduction

Polyvinyl formal (PVF) possesses a number of desirable properties, and is widely used in alpha spectrometry, electron microscopy substrates, and radiation-transparent vacuum windows [1, 2]. PVF presents high elongation, is easy to fabricate, and can be cast into very thin films [3]. Indeed, PVF film has been used as a mechanical support for the fuel capsule within the hohlraum inside the fusion target that is used to achieve thermonuclear ignition in the National Ignition Facility (NIF) [4–6]. The success of experiments performed at the NIF is critically dependent on the positioning of this fuel capsule, and the static and dynamic mechanical properties of the PVF film appear to play a crucial role in this positioning [7].

PVF (also known as "formvar," e.g., formvar 15/96E) is a copolymer of polyvinyl acetal, polyvinyl alcohol, and polyvinyl acetate [8]. Formvar can also be prepared from polyvinyl acetate using an acid-catalyzed reaction involving formaldyde in aqueous media. Altering the acetic acid:water:formaldehyde ratio used during synthesis allows the composition of the monomers within the resulting polymer to be modified in order to maximize material performance [9]. Furthermore, previous investigations have shown that formvar films readily absorb and desorb water and that formvar film strength is reduced by exposure to high humidity levels [10].

Absorbed water greatly influences the structural, electrical, and mechanical properties of polymers [11–14]. The mechanism for the absorption of water by the polymer molecule and the corresponding structure–property relationships are very important factors in the environmental aging of polymers and high-performance composites [15]. It has been suggested that the quantity of absorbed water present at equilibrium is dictated by the available free volume [16, 17]. Another supposition is that water absorption is directly correlated to the molecular formula of the polymer and that equilibrium water concentration is a molar additive function, leading to relationships with some predictive properties [18, 19]. Note that, in all of the studies referenced above, dynamic mechanical analysis as well as calorimetric and dielectric measurements were the main research tools employed.

Molecular simulations can provide insight into the influence of water on the thermal and mechanical properties of polymers. Neyertz et al. [20] studied the effects of different weight percentages of water on the volumetric and energetic properties of a polymer as well as its specific interactions with water, and

Q. Yin · L. Zhang · K. Du (✉)
Research Center of Laser Fusion, China Academy of Engineering Physics, P.O. Box 919-987, Sichuan 621900, China
e-mail: kaidu839@sohu.com

B. Jiang · Q. Yin
College of Chemistry, Sichuan University, Sichuan 610064, China

explored the existence of water clusters as a function of the water content. Goudeau et al. [21] used molecular dynamics simulation to elucidate the effect of water on the structure of the amorphous region of polyamide 6,6, and they found highly localized water organization relative to the polyamide moieties, in qualitative agreement with a two-step sorption model. Wu et al. [22] carried out a series of two-step molecular dynamics simulations to study the effects of moisture on an epoxy–amine polymer network. Simulated results clearly indicated that, upon the addition of water molecules, the density of the polymer system decreased, whereas the mobility of the network chains increased at high water concentrations. Ennari [23] reported the diffusion coefficients of the protons, hydronium ions, and water molecules in sulfonated PVF-based polyelectrolyte materials, and studied the movement of ions by atomistic molecular modeling. Darvas [24] reported the molecular dynamics simulation of poly(ethylene oxide) (PEO) adsorbed at the free surface of water. It was found that the adsorption of PEO at the water's surface was determined by two main competitive processes: the solvation of the segments and the adsorption of the surface-active monomer segments.

In the study reported in the present paper, a series of molecular dynamics simulations were performed to study the effects of water on polyvinyl formal. We studied the changes in the density, fractional free volume, radius of gyration, cohesive energy density, diffusion of water, and radial distribution function as the water content was varied. The model and simulation techniques used are described in the next section. The section after that provides the results and a discussion of them, before conclusions are drawn in the final section.

Model and simulations

MD simulations were performed using the Discover and Amorphous Cell modules of the Accelrys Materials Studio 4.3 simulation software package. Energy minimization was conducted using the smart minimizer method, which switches from the steepest-descent to the conjugated-gradient and then to the Newton method as the energy derivatives decrease, in order to accelerate the computation [25]. For the MD process, the Nose thermostat and Andersen barostat were used to control temperature and pressure, respectively. The Lennard–Jones potential was adopted to model van der Waals interactions. The short-range Lennard–Jones potential was cut off at 9 Å and long-range correction terms were added [26]. The time step was set to 1 fs in all MD runs.

The COMPASS (i.e., condensed-phase optimized molecular potentials for atomistic simulation studies) force field [27] was used throughout the simulations. This ab initio force field enables the properties of the gas phases and condensed phases of a broad range of molecules and polymers to be predicted accurately and simultaneously [28–30]. The COMPASS force field potential is represented as follows [31]:

$$E_{\text{total}} = E_{\text{valence}} + E_{\text{cross-term}} + E_{\text{nonbond}}, \quad (1)$$

where E_{valence} is the valence energy, $E_{\text{cross-term}}$ is the cross-term interaction energy, and E_{nonbond} is the nonbonded interaction energy. Further details of this force field can be found elsewhere [32, 33].

Random PVF copolymers with 100 repeat units (the polyvinyl acetal:polyvinyl alcohol:polyvinyl acetate ratio was 82:12:6) were generated. Energy minimization and geometry optimization of the PVF chains were performed prior to amorphous cell construction.

The initial polymeric conformation was constructed from four chains with 100 repeat units, and the water was randomly embedded into the amorphous cell. To simulate the effect of the water on the PVF membrane, different numbers of water molecules and the four polymer chains with 100 repeat units were constructed with periodic boundary conditions. To prevent ring catenation during model construction, it is usually necessary to start modeling with an unrealistically low initial packing density (typically 0.1 g/cm^3). A summary of the properties generated from the simulations is presented in Table 1.

The initially dense membranes were subsequently optimized by a 10,000-step energy minimization to eliminate irrelevant

Table 1 Properties of the amorphous cell with different numbers of water molecules

	Number of water molecules								
	0	5	10	20	30	40	60	80	100
Number of PVF chains	4	4	4	4	4	4	4	4	4
Number of atoms	5672	5687	5702	5732	5762	5792	5852	5912	5972
Net mass	38036	38126	38216	38396	38576	38756	39116	39476	39836
wt% of water	0	0.23	0.47	0.94	1.40	1.86	2.76	3.65	4.52
Volume (Å^3)	51475	51597	51719	51963	52207	52450	52938	53426	53913

contacts by smart minimization. Afterward, a 500-ps MD equilibration run was performed with the NPT ensemble at 298 K and 101.325 kPa to obtain the equilibrium density using the Discover module. Afterward, using the Forcite module, an MD equilibration run was performed for the final membranes using an annealing procedure and the temperature cycling method. During the annealing, the systems were heated from 298 to 598 K in steps of 50 K and then cooled back down in steps of 50 K. Each annealing step involved a 50-ps simulation with the NPT ensemble. After that, a 20-ns MD equilibration run was implemented for the PVF membranes with the NPT ensemble to obtain the final equilibrium density at 298 K and 101.325 kPa. The atomic trajectory, which was recorded every picosecond, was suitable for analyzing the structural and equilibrium thermodynamic properties of the system. A snapshot of every PVF/water system is shown in Fig. 1. The simulation cells containing 0, 5, 10, 20, 30, 40, 60, 80, and 100 H_2O molecules correspond to the nine concentrations of H_2O, i.e., 0, 0.23, 0.47, 0.94, 1.40, 1.86, 2.76, 3.65, and 4.52 wt%.

Results and discussion

Density

All PVF/water systems were generated with the density of dry amorphous PVF. Due to the influence of the water molecules, the density of the system was expected to change during equilibration under constant-NPT conditions. Three typical curves (for PVF, PVF+0.47 % water, and PVF+

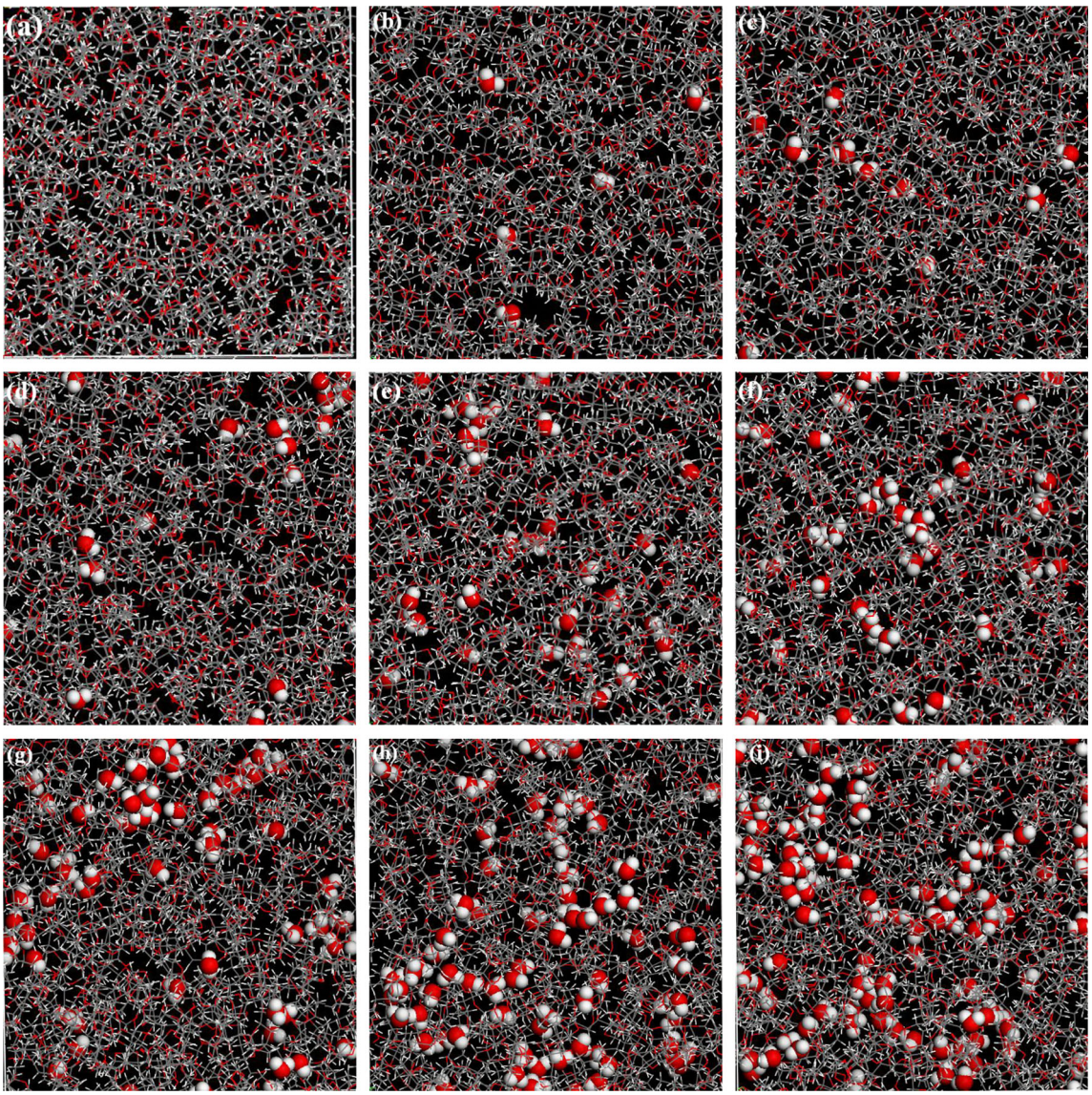

Fig. 1 **a**–**i** Snapshots of simulation cells containing **a** PVF only and **b**–**i** PVF/H_2O systems with different H_2O loadings (0, 5, 10, 20, 30, 40, 60, 80, and 100 H_2O molecules)l. The water molecules are displayed in CPK style so that they can be distinguished from the polymer chain

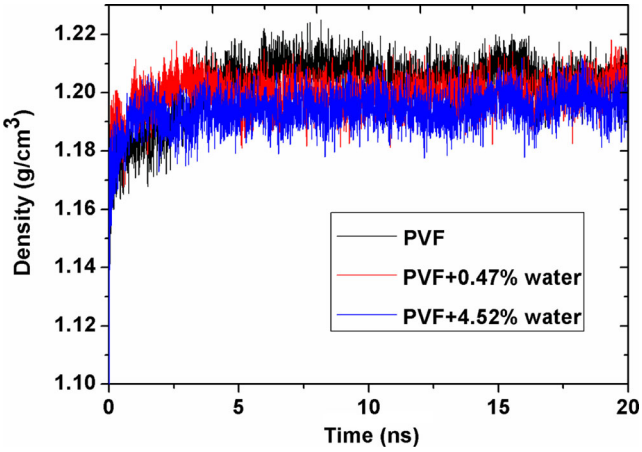

Fig. 2 Density vs time during the equilibration of various PVF-only and PVF/water systems

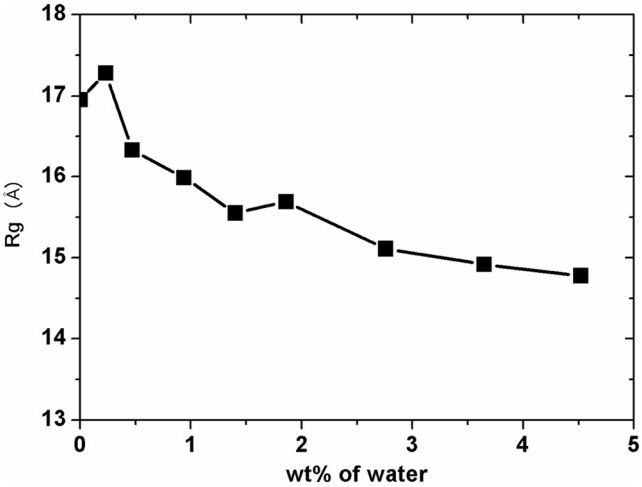

Fig. 4 Radius of gyration *Rg* as a function of the water content (wt%)

4.52 % water) of density vs time during the equilibration are shown in Fig. 2. Because the PVF and PVF/water systems had a low density (typically 0.1 g/cm^3) when generated, the system density in Fig. 2 shows a strong increase during the first 500-ps NpT MD simulation before settling down to a constant level for the rest of the equilibration. In addition, the average PVF membrane density was calculated from the other 19,500 ps of the MD equilibration run for the PVF membranes, performed in the NPT ensemble at 298 K and 101.325 kPa.

The densities of all the PVF/water systems after equilibration are compared in Fig. 3. The simulated density of PVF without water at 298 K and 101.325 kPa was 1.202, in good agreement with the experimental value of 1.23 g/cm^3 obtained from the CAS database (#9003-33-2). These results show that a linear combination rule (by weight fraction) seems to apply to all PVF/water systems investigated, within the precision associated with the density data calculated by MD simulations. The densities of equivalent structures that were generated independently were within 2 % and in the same range as the deviations of the densities of the structures obtained from the linear combination rule.

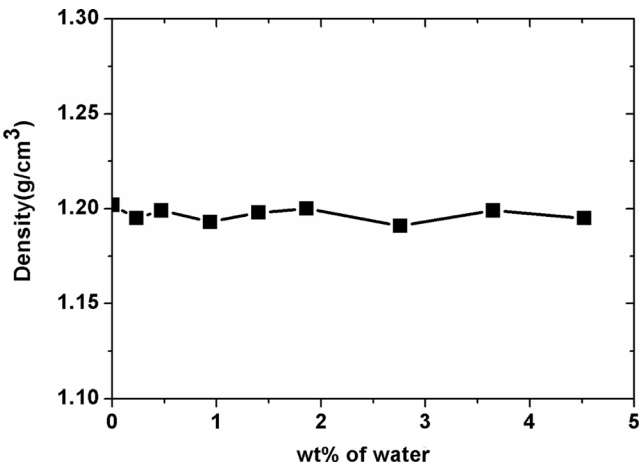

Fig. 3 Densities of PVF/water systems as a function of the water content (wt%)

Radius of gyration

A useful structural parameter to measure the size of the polymer is its radius of gyration, *Rg*, defined as

$$Rg = \sqrt{\frac{\sum_i (|r_i|)^2 m_i}{\sum_i m_i}}, \quad (2)$$

where m_i is the mass of atom i and r_i is the position of atom i with respect to the center of mass of the molecule. An increase in *Rg* indicates polymer expansion, while a decrease in *Rg*

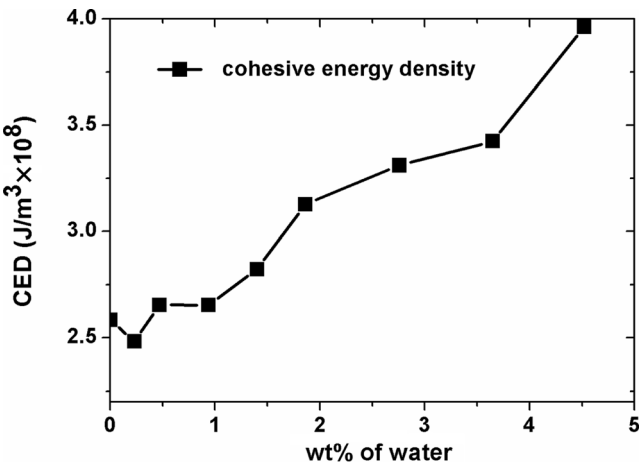

Fig. 5 Cohesive energy density as a function of the water content (wt%)

implies polymer contraction. Figure 4 shows *Rg* as a function of the water content (wt%).

As shown in the figure, the water content has a significant effect on the total polymer size. When the water content is low, the polymer chain adopts an elongated conformation because of the molecular interactions between the polymer chains. The radius of gyration of polyvinyl formal chains decreases with increasing water content. This can be explained as follows. Upon adding water molecules, the affinity of the hydrogen atoms in water for oxygen atoms in the polymer lead to the formation of hydrogen bonds between the water molecules and the polymer chains of PVF, enhancing the rigidity of the polymer and increasing both inter- and intrachain interactions. The increased rigidity of the polymer causes a decrease in its radius of gyration.

Cohesive energy density

The cohesive energy is defined in atomistic simulations as the increase in energy per mole of a material upon eliminating all intermolecular forces [34]. Normalizing the cohesive energy with the molar volume yields the cohesive energy density, which is a measure of the intermolecular forces in a system, estimated via the nonbonded parameters of the force field. Figure 5 presents the cohesive energy density for each of the systems studied here as a function of the water content (wt%). Generally, increasing the water content increased the cohesive energy density of the polymer chain, favoring the formation of intermolecular hydrogen bonds between the water molecules and the polymer chains of PVF. Calculations of the cohesive energy density showed that the presence of water enhances the

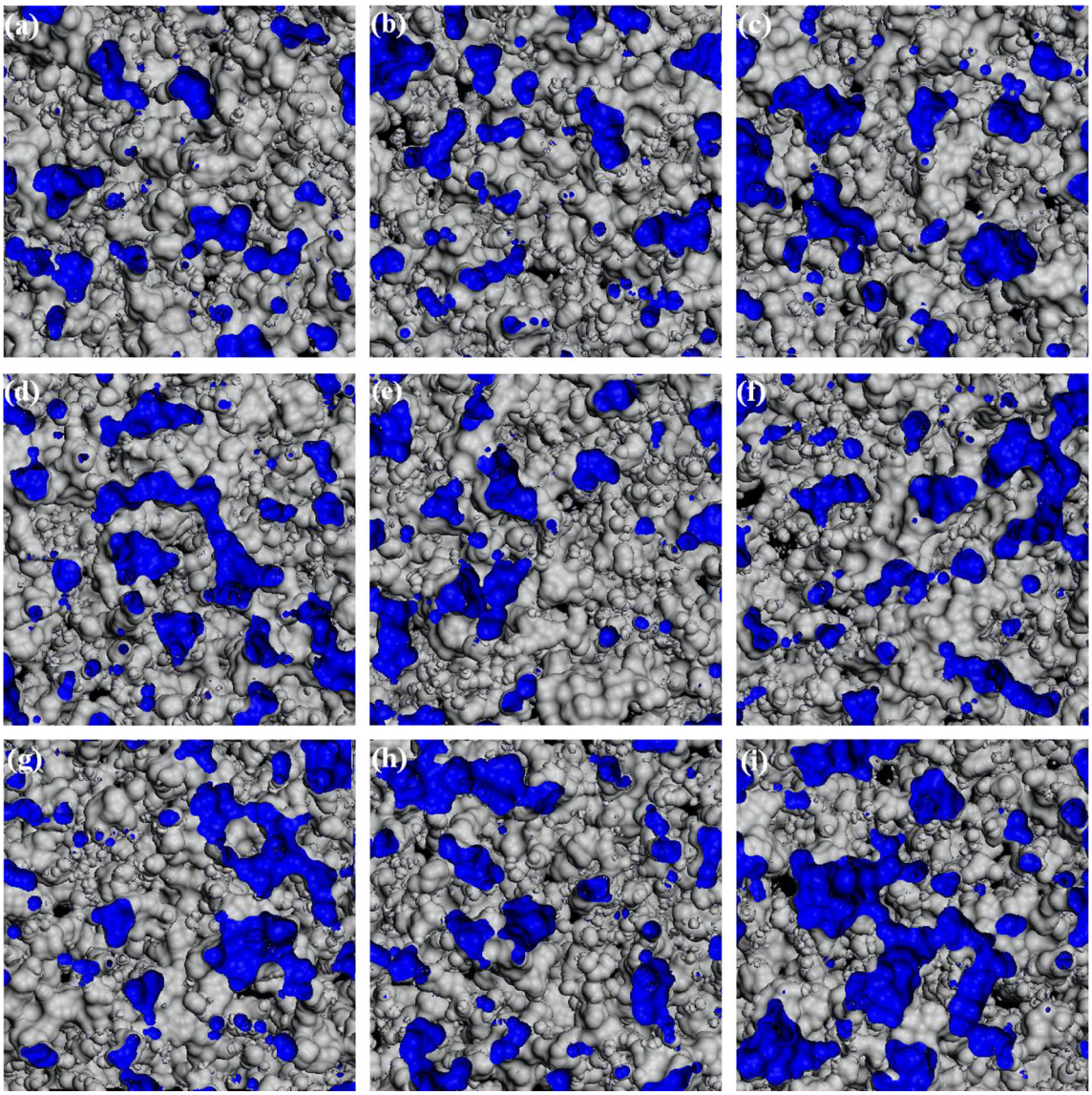

Fig. 6 **a**–**i** Free-volume morphologies in the **a** PVF-only and **b**–**i** PVF/H_2O systems at different H_2O loadings (5, 10, 20, 30, 40, 60, 80, and 100 H_2O molecules in the simulation cell)

intensity of the intermolecular interactions between neighboring macromolecules, mainly because of electrostatic interactions between the water and the polymer chains.

Fractional free volume (FFV)

The size and morphology of the free volume are very important influences on the transport behavior of molecules that penetrate into polymer membranes. The fractional free volume (FFV) is defined as

$$\mathrm{FFV} = \frac{V - V_0}{V} = \frac{V - 1.3V_{\mathrm{W}}}{V}, \tag{3}$$

where V is the specific volume, V_0 is the occupied polymer chain volume, and V_{W} is the van der Waals volume of the polymer chains. Figure 6 illustrates the free-volume morphologies in the PVF-only and PVF/H_2O systems. At low H_2O concentrations, the free volume is dominated by a collection of small voids. However, at high H_2O concentrations, large voids appear, some of which are interconnected.

In the MD simulations, the free volumes of the membranes were also analyzed using the Connolly surface method. The probe molecule was modeled using hard spheres of radius 0.1 nm. The change in the fractional free volume of the PVF membrane as the water content is varied is displayed in Fig. 7. Generally, the fractional free volume of the polymer chain initially decreased with increasing water concentration before increasing beyond a certain water concentration. This can be explained as follows. When a small amount of water is added (<0.5 %), the water molecules appear to be accommodated in the free volume available in the PVF matrix, resulting in a relatively low free volume and a decrease in the available free volume. At relatively high concentrations of water (>0.5 %), the fractional free volume increases slowly below 2 % and then increases rapidly above 2 %. As the concentration of water is increased (<2 %), some of the water molecules are absorbed into the polymer matrix, resulting in minor volumetric swelling of the PVF system, so the fractional free volume slowly increases. However, when more water is absorbed into the polymer matrix (>2 %), there is no remaining free volume to accommodate the extra water molecules. The matrix is therefore saturated with water molecules, so adding more water leads to a rapid increase in the fractional free volume.

Diffusion of water molecules

Since the dynamics of water significantly depend upon its environment, the diffusion of H_2O into the polymers can provide some useful information concerning the structure and properties of the polymer itself. Diffusion coefficients were obtained from the mean squared displacement (MSD) of the penetrating molecules according to Einstein's equation:

$$D_\alpha = \frac{1}{6N_\alpha} \lim_{t\to\infty} \frac{d}{dt} \sum_{i=1}^{N_\alpha} \left\langle [r_i(t) - r_i(0)]^2 \right\rangle, \tag{4}$$

where D is the diffusion coefficient, $r_i(0)$ is the initial coordinates of the penetrating molecule in the polymer microstructure, and $r_i(t)$ is the coordinates of the penetrating molecule after time t. $[r_i(t) - r_i(0)]$ represents the displacement of the penetrating molecule during time t, and N is the total number of penetrating molecules.

The diffusion of water molecules in the polyvinyl formal system was studied by implementing 20-ns NPT MD simulations with different water contents. Plots of the MSD of the water molecules as a function of time are shown in Fig. 8.

According to Eq. 4, a plot of MSD versus time should be linear if D is constant; that is, the water molecules should

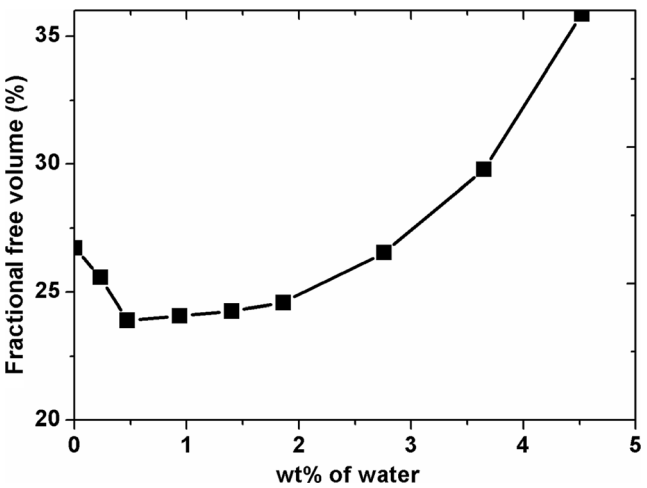

Fig. 7 Fractional free volume as a function of the water content (wt%)

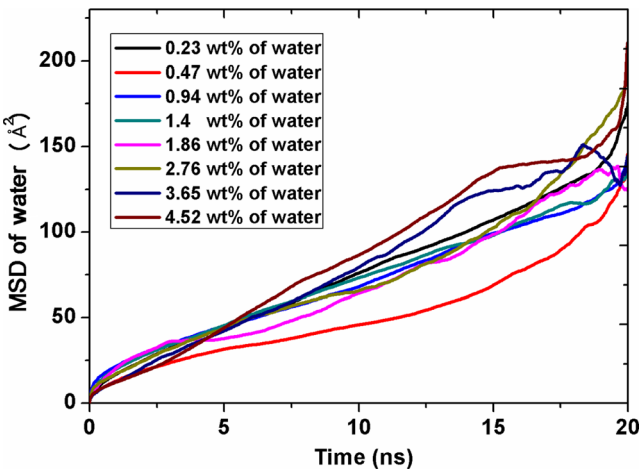

Fig. 8 MSD of water molecules as a function of simulation time (t) for each PVF/water system

exhibit normal (Einstein) diffusion behavior. However, at long times, the plots deviate from linearity due to the increasing statistical error in the MSD calculations [35]. The diffusion coefficients of water molecules at different water contents were calculated from linear fits of plots of MSD versus time, and the results are shown in Fig. 9.

From Fig. 9, the diffusivity of water in the PVF polymer was found to initially decrease and then monotonically increase with increasing water concentration. As the concentration of water increases beyond 0.5 wt%, the diffusion coefficient of water increases. This can be explained by fractional free volume theory as follows. At low water concentrations, the water molecules appear to be accommodated into the available free volume in the PVF matrix, so the mobility of water is confined to the available free volume, meaning that the diffusion coefficient of water decreases. As the concentration is increased, the free volume available to accommodate the new water molecules decreases until the matrix is saturated, which causes the water diffusion coefficient to increase.

Radial distribution function

The radial distribution function (RDF) is a measure of the probability that there is an atom within a spherical shell of infinitesimal thickness at a distance r from a reference atom. The resulting function is denoted $g_{AB}(r)$, and is calculated by averaging over the static relationships between all pairs of particles AB as follows:

$$g_{AB}(r) = \frac{\langle n_{AB}(r) \rangle}{4\pi r^2 \Delta \rho_{AB}}, \quad (5)$$

where $<n_{AB}(r)>$ is the average number of atom pairs between r and $r + \Delta r$, and ρ_{AB} is the density of AB atom pairs. In order to determine the effect of the relative water content on the structure of the PVF polymer, the radial distribution functions of PVF/water mixtures with various water concentrations were obtained via MD simulation.

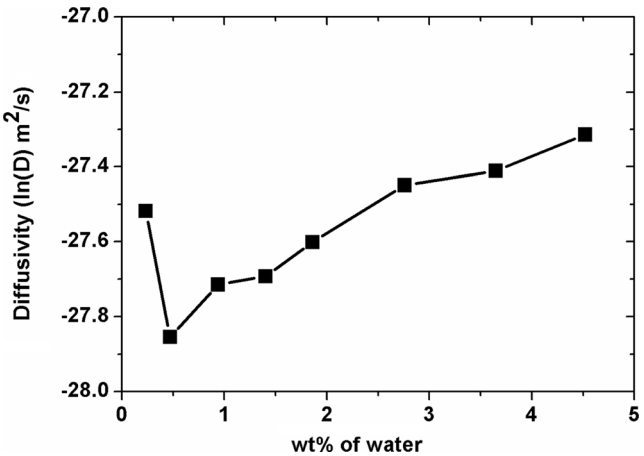

Fig. 9 Diffusion coefficient of water as a function of the water content (wt%)

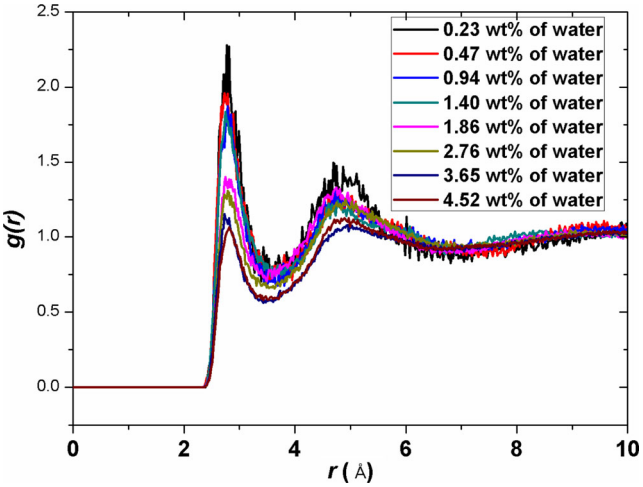

Fig. 10 Intermolecular RDFs for pairs of oxygen atoms (where one of the oxygens is in the polymer and the other is in a water molecule) in polymer/water systems with different water contents

Generally, RDFs can be used to identify the distance associated with the nearest interaction, and can provide important information about the polar interactions between water and polymer networks, such as hydrogen bonding. Figure 10 shows, for polymers with different water contents, the intermolecular RDFs for pairs of oxygen atoms, where one of the oxygens is in the polymer and the other is in a water molecule. All of the PVF/water mixtures display similar peaks at distances of 2.75 Å and 5.07 Å. The sharp peak at 2.75 Å is an indication of the presence of hydrogen bonds, whereas the broap peak at 5.07 Å is associated with the symmetry of polar groups in acetal, alcohol, and acetate moieties in the polymer network. The shorter distance associated with the sharp peak at 2.75 Å indicates that the absorbed water molecules prefer to be located in the vicinity of the polar groups in the polymer network. The concentration of water does not affect the

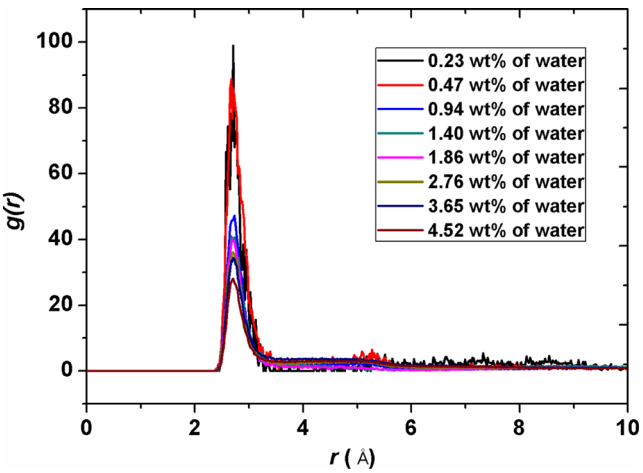

Fig. 11 Intermolecular RDFs between oxygen atoms in water molecules present in polymer/water systems with different water contents

positions of the peaks and valleys in the RDFs, only their heights and depths. It can be seen that the probability of hydrogen-bond formation drops monotonically with increasing water concentration. This is because the number of polar groups available for hydrogen bonding in the network does not change upon the addition of water molecules, and when these polar groups are all hydrogen-bonded to water molecules, any water molecules that are not hydrogen-bonded to polar groups prefer to form hydrogen bonds with other water molecules, not with the polar groups in the network. This indicates that water molecule clusters appear at higher water concentrations.

In addition to this analysis, the intermolecular RDFs between oxygen atoms in water molecules were evaluated for polymer/water systems with different water contents. These RDFs are shown in Fig. 11. It can be seen that the RDFs for all water concentrations show a sharp peak at a distance of 2.80 Å, indicating self-aggregation of water molecules. The probability of self-aggregation drops monotonically as the water content increases from 0.23 wt% to 4.52 wt%. This is further proof that water molecules tend to cluster together at higher water concentrations, which is consistent with the results of simulations of other polymer systems reported by Wu et al. [22].

Conclusions

Molecular dynamics simulations afforded clear results for the density, radius of gyration, cohesive energy density, fractional free volume, diffusion of water molecules, and radial distribution function of each PVF/water system studied in this work. The radius of gyration of the polymer chain was found to decrease whereas the cohesive energy density increased as the concentration of water molecules was increased. The incorporation of water molecules enhances the intensity of intermolecular interactions between neighboring macromolecules. The polymer chains form hydrogen bonds with absorbed water molecules, which prefer to be located in the vicinity of polar groups in the polymer chains. The MD simulations also indicated that the diffusion coefficient of water initially decreases with increasing water concentration before increasing when the water concentration passes a critical value. The same trend was observed for the fractional free volume. We can therefore conclude that the water molecules are accommodated in the available free volume in the polyvinyl formal matrix at low concentrations, resulting in a decrease in the free volume available to a molecule diffusing into the system. However, as the concentration of water increases, volumetric swelling of the polymer matrix occurs.

References

1. Rusu OA, Dreve SR, Begy CD (2011) Characteristics of formvar films used to prevent alpha-detector contamination. J Radioanal Nucl Chem 290:241–245
2. Popil R, Gupta PD, Fedosejevs R, Offenberger A-A (1987) Measurement of KrF-laser-plasma X-ray radiation from targets with various atomic numbers. Phys Rev A 35:3874–3882
3. Stadermann M, Kucheyev SO, Lewicki J, Letts SA (2012) Radiation tolerance of ultra-thin formvar films. Appl Phys Lett 101:071908
4. Haan SW, Atherton J, Clark DS (2013) NIF ignition campaign target performance and requirements: status May 2012. Fusion Sci Technol 63:67–75
5. Haan SW (2011) Point design targets, specifications, and requirements for the 2010 ignition campaign on the National Ignition Facility. Phys Plasmas 18:051001
6. Miller GH, Moses EI, Wuest CR (2004) The National Ignition Facility. Opt Eng 443:2841
7. Stadermann M, Letts SA, Bhandarkar S (2011) Improvements to formvar tent fabrication using the meniscus coater. Fusion Sci Technol 59:58–62
8. Stadermann M (2010) Formvar tents for NIF targets. In: 19th Target Fabrication Meeting, Orlando, FL, USA, 21–26 Feb 2010
9. Miller PE, Stadermann M, Suratwala TI (2012) The influence of chemical and mechanical effects on the stability and strength of formvar tents. In: 20th Target Fabrication Meeting, Santa Fe, NM, 20–24 May 2012
10. Stadermann M, Fair J, Letts SA, Feit M, Suratwala TI (2012) Environmental effects on tent processing and tent stability in NIC targets. In: 20th Target Fabrication Meeting, Santa Fe, NM, 20–24 May 2012
11. Han SO, Drzal LI (2003) Water absorption effect on hydrophilic polymer matrix of carboxyl fuctionalized glucose resion and epoxy resin. Eur Polym J 39:1791–1799
12. Deligöz H, Yalcinyuva T, Özgümüs S, Yildirim S (2006) Electrical properties of conventional polyimide films: Effect of chemical structure and water uptake. J Appl Polym Sci 100:810–818
13. Kim HJ, Seo DW (2006) Effect of water absorption fatigue on mechanical properties of sisal textile-reforced composites. Int J Fatigue 28:1307–1314
14. Dhakal HN, Zhang ZY, Richardson MOW (2007) Effect of water absorption on the mechanical properties of hemp fibre reinforced unsaturated polyester composites. Compos Sci Technol 67:1674–1683
15. Merdasa I, Tcharkhtchia A, Thominettea F, Verdua J, Deanb K, Cookb W (2002) Water absorption by uncrosslinked polymers, networks and IPNs having medium to high polarity. Polymer 43:4619–4625
16. Poliks MD, Schaefer J (1990) Characterization of the chain dynamics of PEEK by CPMAS carbon-13 NMR. Macromolecules 23:3426–3431
17. Clark JN, Jagannathan NR, Herring FG (1988) A nuclear magnetic resonance study of poly(aryl ether ether ketone). Polymer 29:341–345
18. Morel E, Bellenger V, Verdu J (1985) Structure–water absorption relationships for amine-cured epoxy resins. Polymer 26: 1719–1724
19. Bellenger V, Verdu J, Morel E (1989) Structure–properties relationships for densely crosslinked epoxide–amine systems based on epoxide or amine mixture. Part 2. Water absorption and diffusion. J Mater Sci 24:63–68
20. Marque G, Neyertz S, Verdu J, Prunier V (2008) Molecular dynamics simulation study of water in amorphous kapton. Macromolecules 41: 3349–3362

21. Sylvain G, Magali C, Caroll V, Florian MP (2004) Atomistic simulation of the water influence on the local structure of polyamide 6,6. Macromolecules 37:8072–8081
22. Wu CF, Xu WJ (2007) Atomistic simulation study of absorbed water influence on structure and properties of crosslinked epoxy resin. Polymer 48:5440–5448
23. Ennari J (2008) Modelling of transport properties and state of water of polyelectrolytes containing various amounts of water. Polymer 49: 2373–2380
24. Darvas M, Gilanyi T, Jedlovszky P (2010) Adsorption of poly(ethylene oxide) at the free water surface. A computer simulation study. J Phys Chem B 114:10995–11001
25. Pan FS, Peng FB, Jiang ZY (2007) Diffusion behavior of benzene/cyclohexane molecules in poly(vinyl alcohol)-graphite hybrid membranes by molecular dynamics simulation. Chem Eng Sci 62: 703–710
26. Allen MP, Tildesley DJ (1987) Computer simulation of liquids. Oxford University Press, Oxford, p 64
27. Sun H (1998) COMPASS: An ab initio force-field optimized for condensedphase applications overview with details on alkane and benzene compounds. J Phys Chem B 102:7338–7364
28. Chen ZX, Gu Q, Zou HF, Zhao TQ, Wang HY (2007) Molecular dynamics simulation of water diffusion inside an amorphous polyacrylate latex film. J Polym Sci Part B Polym Phys 45:884–891
29. Mahmoud R, Hamid M, Reza G (2012) Molecular simulation study of polyurethane membranes. Polymer 53:1939–1950
30. Wang Q, Keffer DJ, Petrovan S, Thomas JB (2010) Molecular dynamics simulation of poly(ethylene terephthalate) oligomers. J Phys Chem B 114:786–795
31. Wang LZ, Duan LL (2012) Isothermal crystallization of a single polyethylene chain induced by graphene: a molecular dynamics simulation. Comput Theor Chem 1002:59–63
32. Tack JL, Ford DM (2008) Thermodynamic and mechanical properties of epoxy resin DGEBF crosslinked with DETDA by molecular dynamics. J Mol Graph Model 26:1269–1275
33. Grujicic M, Cao G, Roy WN (2004) Atomistic modeling of solubilization of carbon nanotubes by non-covalent functionalization with poly(*p*-phenylenevinyleneco-2,5-dioctoxy-*m*-phenylenevinylene). Appl Surf Sci 227:349–363
34. Bernd K, Michael E, Reinhart A (1996) Atomistic modeling of amorphous polymer bulk based on an ab initio optimized force field. Macromolecules 29:4051–4059
35. Chang SH, Kim HS (2011) Investigation of hygroscopic properties in electronic packages using molecular dynamics simulation. Polymer 52:3437–3442